NAVAL POSTGRADUATE SCHOOL

MONTEREY, CALIFORNIA

THESIS

MOMENTUM EXCHANGE NEAR ICE KEELS IN THE UNDER ICE OCEAN BOUNDARY LAYER

by

John Charles Bleidorn

March 2008

Thesis Advisor: Timothy Stanton
Second Reader: William Shaw

Approved for public release; distribution is unlimited

THIS PAGE INTENTIONALLY LEFT BLANK

REPORT DOCUMENTATION PAGE			Form Approved OMB No. 0704-0188
Public reporting burden for this collection of information is estimated to average 1 hour per response, including the time for reviewing instruction, searching existing data sources, gathering and maintaining the data needed, and completing and reviewing the collection of information. Send comments regarding this burden estimate or any other aspect of this collection of information, including suggestions for reducing this burden, to Washington headquarters Services, Directorate for Information Operations and Reports, 1215 Jefferson Davis Highway, Suite 1204, Arlington, VA 22202-4302, and to the Office of Management and Budget, Paperwork Reduction Project (0704-0188) Washington DC 20503.			
1. AGENCY USE ONLY ***(Leave blank)***	**2. REPORT DATE** March 2008	**3. REPORT TYPE AND DATES COVERED** Master's Thesis	
4. TITLE AND SUBTITLE Momentum Exchange Near Ice Keels in the Under Ice Ocean Boundary Layer		**5. FUNDING NUMBERS**	
6. AUTHOR(S) John Charles Bleidorn			
7. PERFORMING ORGANIZATION NAME(S) AND ADDRESS(ES) Naval Postgraduate School Monterey, CA 93943-5000		**8. PERFORMING ORGANIZATION REPORT NUMBER**	
9. SPONSORING /MONITORING AGENCY NAME(S) AND ADDRESS(ES) N/A		**10. SPONSORING/MONITORING AGENCY REPORT NUMBER**	
11. SUPPLEMENTARY NOTES The views expressed in this thesis are those of the author and do not reflect the official policy or position of the Department of Defense or the U.S. Government.			
12a. DISTRIBUTION / AVAILABILITY STATEMENT Approved for public release; distribution is unlimited		**12b. DISTRIBUTION CODE**	

13. ABSTRACT (maximum 200 words)

This thesis describes momentum exchange in the under-ice ocean boundary layer near ice keels. Understanding ice-ocean momentum exchange is important for accurate predictive ice modeling. Due to climate change, increased naval presence in the Arctic region is anticipated and ice models will become necessary for tactical and safety reasons. Measurements took place in March 2007 in the Beaufort Sea at the Applied Physics Laboratory Ice Station sponsored by the U.S. Navy.

Turbulence measurements were made at a single point behind a large multi-year ice ridge in the upper ocean boundary layer. The keel was found to be at least 12.5m deep and much broader than expected. Ocean profiles showed the pycnocline between 13-18m deep and thus a unique situation of measuring the flow around a large ice structure in a shallow boundary layer presented itself.

Results indicate that estimates of turbulence intensity depend on ice speed, direction and measurement depth. Velocity spectra indicate periods of low inertial subrange levels likely resulting from close proximity to the pycnocline. Low frequency variance in the velocity spectra was also observed and is thought to be a wake effect resulting from an under ice structure upstream of the flow.

14. SUBJECT TERMS Arctic, momentum exchange, under-ice, ice keels, Reynolds stress, turbulence			**15. NUMBER OF PAGES** 51
			16. PRICE CODE
17. SECURITY CLASSIFICATION OF REPORT Unclassified	**18. SECURITY CLASSIFICATION OF THIS PAGE** Unclassified	**19. SECURITY CLASSIFICATION OF ABSTRACT** Unclassified	**20. LIMITATION OF ABSTRACT** UU

NSN 7540-01-280-5500 Standard Form 298 (Rev. 2-89)
Prescribed by ANSI Std. 239-18

THIS PAGE INTENTIONALLY LEFT BLANK

Approved for public release; distribution is unlimited

MOMENTUM EXCHANGE NEAR ICE KEELS IN THE UNDER ICE OCEAN BOUNDARY LAYER

John C. Bleidorn
Lieutenant, United States Navy
B.S., U.S Naval Academy, Annapolis, 1999

Submitted in partial fulfillment of the
requirements for the degree of

MASTER OF SCIENCE IN METEOROLOGY AND PHYSICAL OCEANOGRAPHY

from the

NAVAL POSTGRADUATE SCHOOL
March 2008

Author: John Charles Bleidorn

Approved by: Timothy Stanton
Thesis Advisor

William Shaw
Second Reader

Mary Batteen
Chairman, Department of Oceanography

THIS PAGE INTENTIONALLY LEFT BLANK

ABSTRACT

This thesis describes momentum exchange in the under-ice ocean boundary layer near ice keels. Understanding ice-ocean momentum exchange is important for accurate predictive ice modeling. Due to climate change, increased naval presence in the Arctic region is anticipated and ice models will become necessary for tactical and safety reasons. Measurements took place in March 2007 in the Beaufort Sea at the Applied Physics Laboratory Ice Station sponsored by the U.S. Navy.

Turbulence measurements were made at a single point behind a large multi-year ice ridge in the upper ocean boundary layer. The keel was found to be at least 12.5m deep and much broader than expected. Ocean profiles showed the pycnocline between 13-18m deep and thus a unique situation of measuring the flow around a large ice structure in a shallow boundary layer presented itself.

Results indicate that estimates of turbulence intensity depend on ice speed, direction and measurement depth. Velocity spectra indicate periods of low inertial subrange levels likely resulting from close proximity to the pycnocline. Low frequency variance in the velocity spectra was also observed and is thought to be a wake effect resulting from an under ice structure upstream of the flow.

THIS PAGE INTENTIONALLY LEFT BLANK

TABLE OF CONTENTS

THIS PAGE INTENTIONALLY LEFT BLANK

LIST OF FIGURES

ACKNOWLEDGMENTS

This research was supported by the National Science Foundation under grant ARC-0632041. I would also like to gratefully acknowledge the U.S. Navy Arctic Submarine Laboratory and the University of Washington Applied Physics Laboratory for their invitation to participate in APLIS 2007 and continued support before, during and following the camp. Their assistance and advice enabled this ambitious venture and was instrumental in overcoming the many challenges we experienced along the way.

I also thank the Naval Postgraduate School's Department of Oceanography, particularly Professor Tim Stanton for offering me the opportunity to participate in this exciting experiment, his generous loan of instruments and survival gear necessary for such an undertaking, and his guidance through the thesis process; Dr. William Shaw, whose exceptional patience and instruction kept this project on track, and Commander Denise Kruse who spent countless hours cutting through red tape on our behalf.

Additional gratitude is due to my partner on the ice, LT Tim McGeehan, whose wisdom, friendship, and humor made this an adventure to remember; my mentor, CAPT Scott Katz, who is always ready with words of encouragement and perspective, and most importantly, my wife Amy, whose counsel and love continue to provide faithful guidance throughout my life.

THIS PAGE INTENTIONALLY LEFT BLANK

I. INTRODUCTION

A wide range of physical processes must be described correctly in order to accurately model Arctic Ocean ice formation, melting and motion. The inaccessibility and harsh environment of the Polar Regions has limited the measurement of these processes. If the Arctic regions continue to warm, as some scientists have forecasted, it is conceivable that over the next 10 to 30 years the Arctic Ocean could develop a navigable sea lane for at least part of the year (Whelan et al, 2007). If that becomes a reality, significantly shortened transit routes would reduce shipping costs worldwide. Additionally, abundant mineral resources in the Arctic could become accessible. Growing political tensions in the region over this potential wealth are already being realized and U.S. and allied maritime forces will likely be required to maintain constant patrols in the region. Therefore maritime safety, naval operations, and economic concerns will necessitate a requirement for accurate predictive coupled ocean-ice modeling in this rapidly changing environment.

The way the ice pack exchanges momentum with the atmosphere and ocean as the large scale wind forces it across the sea surface is important for ice modelers. On the ocean side, momentum exchange occurs through turbulent eddies in the under-ice ocean boundary layer. These eddies are formed as wind forced ice drags over the ocean. How much drag the ocean exerts on the ice for a given ice speed is critical to modeling ice movement and can be characterized as a drag coefficient. This ocean-ice drag coefficient is dependent on under-ice roughness, which is highly variable, ranging from very smooth surfaces under frozen leads to massive ice ridge keels that may extend in excess of 50 meters below sea level. Ice keels formed by pressure ridging are thought to be a significant source of under ice drag, particularly if they extend into the stratified part of the water column. Pressure ridges form when synoptic scale convergent winds deform ice floes and are typically 0.5 to 5m high with corresponding keels 3 to 4 times that deep.

In an effort to measure the momentum exchange near an ice keel, detailed turbulence measurements were made at a point 15 meters horizontally from the base of a

pressure ridge at the Applied Physics Laboratory Ice Station (APLIS) 2007. The purpose of this work is to present under ice turbulence data collected during APLIS 2007 and discuss the effects of a large ice keel on the sub-ice flow.

II. BACKGROUND

Air sea interaction in the Arctic is complicated by the presence of the frozen sea surface. To accurately forecast ice movement, the way wind imparts momentum to the ocean through the ice must be understood. Assuming that forces resulting in ice deformation are small, which is widely true far from the land, the shear stress that the wind imparts to the surface ice is equal and opposite to the shear stress that the ocean imparts on the underside of the ice. Given surface wind information and a good understanding of surface ice roughness, it is possible to model wind stress exerted on the ice by a drag law:

$$\tau_{wind} = \rho_{air} C_{D10} U_{10}^2 = \tau_{ice/ocn} . \tag{0.1}$$

Where τ_{wind} and $\tau_{ice/ocn}$ is the stress the ocean and wind imparts on the ice respectively, ρ_{air} is the air density, C_{D10} is a drag coefficient for the ice calculated from 10m winds and U_{10} is the 10m wind speed. Similarly,

$$\tau_{ice/ocean} = \rho_{water} C_{Docn} U_{ocn}^2 , \tag{0.2}$$

where ρ_{water} is the density of salt water, C_{Docn} is a drag coefficient for the ice and U_{ocn}^2 is the ocean current relative to the ice. Knowledge of under ice roughness and upper ocean boundary layer as well as the wind stress on the ice are needed to determine and forecast ice velocity.

A. REYNOLDS STRESSES

Under-ice roughness and ice motion produces turbulent eddies that result in a net downward transfer of momentum, which can be described by manipulation of the advective terms of the instantaneous momentum equations,

$$\frac{\partial u}{\partial t} + u\frac{\partial u}{\partial x} + v\frac{\partial u}{\partial y} + w\frac{\partial u}{\partial z} - fv = -\frac{1}{\rho_o}\frac{\partial \rho}{\partial x} + \upsilon \nabla^2 u \tag{0.3}$$

$$\frac{\partial v}{\partial t} + u\frac{\partial v}{\partial x} + v\frac{\partial v}{\partial y} + w\frac{\partial v}{\partial z} + fu = -\frac{1}{\rho_o}\frac{\partial \rho}{\partial y} + \upsilon \nabla^2 v \tag{0.4}$$

$$\frac{\partial w}{\partial t}+u\frac{\partial w}{\partial x}+v\frac{\partial w}{\partial y}+w\frac{\partial w}{\partial z}=-\frac{1}{\rho_o}\frac{\partial \rho}{\partial z}+\upsilon\nabla^2 w. \tag{0.5}$$

By assuming that variables in the momentum equations consist of a slowly-varying component and higher frequency turbulent perturbation component, then decomposing the velocity components *u*, *v*, and *w* into mean flow (indicated by overbar variables) plus a perturbation (indicated by the primed variables);

$$u=\bar{u}+u' \tag{0.6}$$

$$v=\bar{v}+v' \tag{0.7}$$

$$w=\bar{w}+w', \tag{0.8}$$

applying the continuity equation,

$$\frac{du}{dx}+\frac{dv}{dy}+\frac{dw}{dz}=0, \tag{0.9}$$

Then by Reynolds averaging, the Reynolds-averaged momentum equations are derived,

$$\frac{\partial \bar{u}}{\partial t}+\bar{u}\frac{\partial \bar{u}}{\partial x}+\bar{v}\frac{\partial \bar{u}}{\partial y}+\bar{w}\frac{\partial \bar{u}}{\partial z}-f\bar{v}=-\frac{1}{\rho_o}\frac{\partial \bar{\rho}}{\partial x}+\upsilon\nabla^2\bar{u}-\frac{\partial}{\partial x}(\overline{u'u'})-\frac{\partial}{\partial y}(\overline{u'v'})-\frac{\partial}{\partial z}(\overline{u'w'}) \tag{0.10}$$

$$\frac{\partial \bar{v}}{\partial t}+\bar{u}\frac{\partial \bar{v}}{\partial x}+\bar{v}\frac{\partial \bar{v}}{\partial y}+\bar{w}\frac{\partial \bar{v}}{\partial z}+f\bar{u}=-\frac{1}{\rho_o}\frac{\partial \bar{\rho}}{\partial y}+\upsilon\nabla^2\bar{v}-\frac{\partial}{\partial x}(\overline{v'u'})-\frac{\partial}{\partial y}(\overline{v'v'})-\frac{\partial}{\partial z}(\overline{v'w'}) \tag{0.11}$$

$$\frac{\partial \bar{w}}{\partial t}+\bar{u}\frac{\partial \bar{w}}{\partial x}+\bar{v}\frac{\partial \bar{w}}{\partial y}+\bar{w}\frac{\partial \bar{w}}{\partial z}=-\frac{1}{\rho_o}\frac{\partial \bar{\rho}}{\partial z}+\upsilon\nabla^2\bar{w}-\frac{\partial}{\partial x}(\overline{w'u'})-\frac{\partial}{\partial y}(\overline{w'v'})-\frac{\partial}{\partial z}(\overline{w'w'}) \tag{0.12}$$

where the last three terms are the Reynolds stress terms.

Except in a thin layer adjacent to the boundary, direct frictional effects are small, and the majority of momentum transfer is due to turbulence. It is also true that the wind forced ice speed is much larger than horizontal ocean currents which generates high shear near the ice-ocean interface. Therefore, from the Reynolds-stress terms $\overline{u'w'}$ and $\overline{v'w'}$, it is seen that positive fluctuations of u' and v' are transported downward by negative values of w' while positive values of w' move negative values of u' and v' upward. The result is a net downward transport of momentum. The Reynolds stresses are defined as:

$$\tau_{uw} = -\rho_0 \overline{u'w'} \tag{0.13}$$

$$\tau_{vw} = -\rho_0 \overline{v'w'} \tag{0.14}$$

The magnitude of these stresses, τ_0, is related to the friction velocity, u_* by

$$u_* = \sqrt[4]{\left(\overline{u'w'}\right)^2 + \left(\overline{v'w'}\right)^2} = \sqrt{\frac{\tau_0}{\rho_0}}. \tag{0.15}$$

B. ICE OCEAN BOUNDARY LAYER

In a well-mixed ocean and with a relatively smooth ice cover, with centimeter scale roughness elements, boundary layer depth is limited by rotation to the Ekman Depth, D_E. It is useful to consider the upper ocean boundary layer broken into an inner layer and outer layer. In the inner layer, the size of turbulent eddies is determined only by the distance from the boundary (z) and the roughness length, z_0. The eddy velocity scales with the surface friction velocity u_{*o}. In the outer layer, Coriolis force limits the growth of turbulent eddies with the Ekman depth scale exerting control on the size of the eddies. The boundary layer depth may be further limited by the presence of stratification and therefore defined by the depth of stratification at the base of the surface well mixed layer. Between these inner and outer layers is an overlap layer where the only significant length scale is the interface friction velocity, u_{*o}. Based on dimensional analysis then, the horizontal shear in the overlap layer should be proportional to the friction velocity over the depth:

$$\frac{du}{dz} \sim \frac{u_{*o}}{z}. \tag{0.16}$$

By introducing von Karmen's constant k, the Law of the Wall is derived

$$\frac{du}{dz} = \frac{1}{k}\frac{u_{*o}}{z}, \tag{0.17}$$

and therefore, by integration, the vertical velocity profile is

$$u(z) = \frac{u_{*o}}{k} \ln \frac{z}{z_0}, \tag{0.18}$$

where z_0 is the roughness length and results from defining the integration constant as $-\ln z_0$. In this overlap layer, the stress (i.e. u_*) is assumed to be constant, and thus the velocity profile logarithmic.

In the ice-ocean boundary layer, the roughness on the under ice surface plays a significant role in the boundary layer structure. A potentially significant roughness effect is from ice keels, which can be highly variable in size. Bourke and McLaren (1992) found that ice keels tend to average between 4-6m, increasing in draft near the coastline with maximum keel drafts occasionally exceeding 20m. To describe the effect of large ice keels on the flow, it may be helpful to consider the under ice surface with its own roughness parameter then add larger roughness elements spaced on that surface to represent ice keels. These large elements will have their own form drag associated with them. As a result, the total stress the ocean exerts on the ice can be described as the sum of the skin friction and the form drag associated with the larger roughness elements (Marshall, 1971). Figure (1), taken from Arya (1975), shows how a large roughness element, such as an ice keel formed by pressure ridging, may form separate regions of flow in the under ice ocean boundary layer. Arya (1975) used it for the case of atmospheric boundary layer on top of ice. The under-ice case is roughly analogous, but there may be issues if it is found that adequate scale separation does not exist in the ice-ocean boundary layer, such that the overall roughness length is not significantly smaller than the mixed layer or Ekman depth.

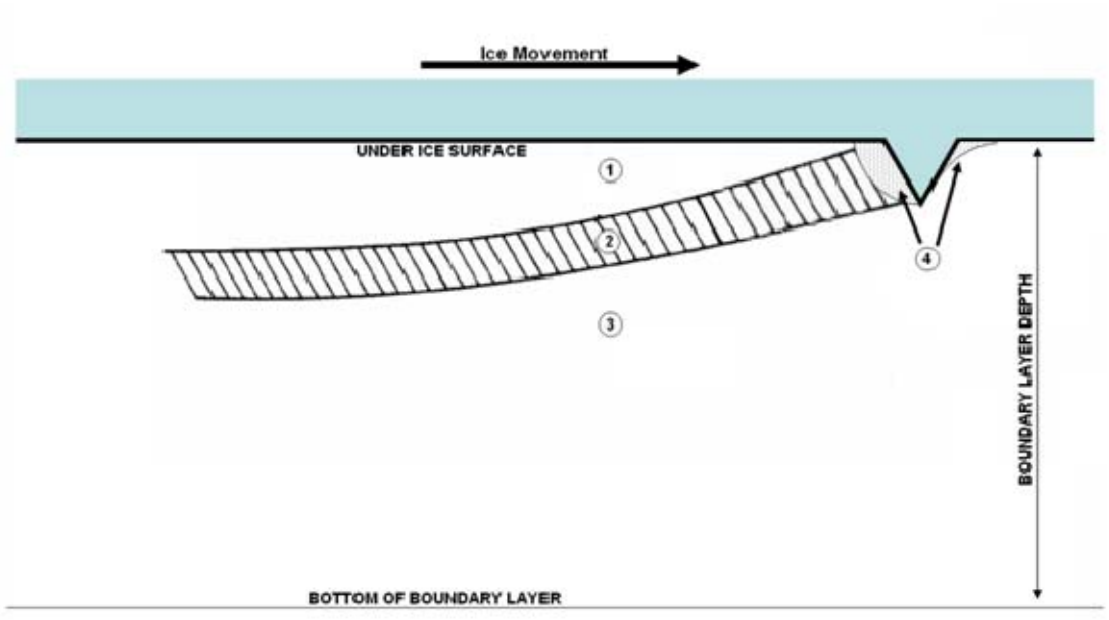

Figure 1. Schematic of under-ice boundary layer adapted from Arya (1975). Flow regions near a single large roughness element surrounded by a relatively smooth ice surface are shown. The four zones of flow (numbered) are described in the text.

In zone 1, the stress is almost entirely due to the roughness of the relatively flat under ice surface. The stress in zone 3 is characterized by a combination of the effects of the large roughness element as well as the surrounding surface. Zone 4 represents regions of separated flow both in front and behind large roughness elements where very low stresses are present. Zone 2 is the turbulent wake associated with the large element and in effect is a blending region for zones 1 and 3. This region will eventually merge with the main boundary layer far from the roughness element. Additionally, zone 3 is expected to have characteristics associated with a typical boundary layer, including a layer where the velocity profile is logarithmic beginning at some distance below the large scale roughness element given by:

$$u(z) = \frac{U_*}{k} \ln\left(\frac{z}{Z_0}\right) \tag{0.19}$$

where U_* is the large scale friction velocity, z is the distance from the ice and Z_0 is the overall roughness length for the field of ice keels (Arya, 1975). Therefore, by measuring

the velocity profile behind a large roughness element and estimating Reynolds stresses at that depth, the large scale roughness length can be determined which is an important parameter for large scale modelers.

III. INSTRUMENTS

A suite of instruments were shipped to the ice camp prior to arrival. Instruments sent to the site measured under-ice three component velocity, temperature and salinity profiles, ice movement, topside ice topography, meteorological conditions, and under-ice morphology.

A. ACOUSTIC DOPPLER VELOCIMETER

Turbulent velocity fluctuations were derived from current measurements made by a SONTEK Acoustic Doppler Velocimeter (ADV). Two ADVs were deployed to the ice, but due to a malfunction, only one was operational during the camp. The ADV provided high resolution currents at 4 Hz. Output variables from the ADV included 3 dimensional currents, corresponding backscatter amplitude, Doppler correlation levels and heading, pitch and roll of the sensor head. The ADV was mounted to an extendable aluminum pole made up of 2.5m segments. The pole, held in place over the ice hole by a tripod, provided for the ADV a rigid mount just below the bottom of the ice. In this way, depth below the ice could be adjusted by adding or removing pole segments as desired.

B. GLOBAL POSITIONING SYSTEM

Ice movement was measured by a handheld Garmin GPS. The unit was mounted on the hut that sheltered the hole through the ice flow. It recorded position at 1 Hz. GPS recorded positions were converted to UTM coordinates, interpolated, and smoothed to yield ice velocity with accuracy greater than 0.05 m/s. An additional GPS receiver was mounted at the Navy command hut approximately 100m away and long term averaged position was used to determine ice rotation, which was found to be negligible during the observation period.

C. WEATHER INSTRUMENTS

Weather data including time stamped 10m wind, temperature and atmospheric pressure measurements were provided by the University of Washington Applied Physics Laboratory (APL) from a Coastal Climate WeatherPak WP-100 automated electronic weather station.

D. TOPSIDE SURVEY

The pressure ridge corresponding to the selected ice keel was surveyed using a leveling rod and a site level mounted on a tripod. Three parallel transects were made running over the ridge to determine changes in height with distance. The measurements yielded accurate dimensions of the top of the pressure ridge from which estimates of the keel are inferred assuming local hydrostatic equilibrium of the ice sheet and keel.

E. OCEAN PROFILES

A SBE 19-03 SEACAT conductivity, temperature and depth recorder was brought with the intention of taking frequent upper ocean profiles throughout the experiment. Because of constant U.S. Navy and British submarine exercises in the area, deployment of instruments below the ice was strictly restricted and no ocean profiles were made from the selected location for the experiment.

University of Washington APL provided temperature and salinity profiles taken with a similar SBE 19 SEACAT Profiler. The profiles were taken from a separate hole located approximately 100m from the ridge from where the turbulence data was measured. Temperature, salinity and depth measurements from the profiler were converted to density profiles using the equation of state as defined by the Joint Panel on Oceanographic Tables and Standards (UNESCO, 1981). Only 10 casts were made throughout the two week period and only three of these casts correspond to the time period during which turbulence data was collected. These three profiles provided the only information regarding mixed layer depth for the experiment.

F. UNDER ICE MORPHOLOGY

A high frequency narrow beam SONAR was brought to image the selected ice keel, but noise problems limited the maps to a 5-7m radius. However, areas of the ice floe were acoustically imaged by both the U.S and British submarines during the ice camp. It is expected that this data will become available for future studies and will include imagery of the ice keel that is central to this experiment.

THIS PAGE INTENTIONALLY LEFT BLANK

IV. DATA COLLECTION

Data collection took place at the Applied Physics Laboratory Ice Station (APLIS) from 15 March to 30 March 2007 by a team from the Naval Postgraduate School Oceanography Department comprised of Navy Lieutenants Timothy McGeehan and John Bleidorn. The APLIS ice camp was established and managed by the University of Washington's Applied Physics Laboratory personnel for the U.S. Navy submarine exercises. The camp was located approximately 300 km north of Prudhoe Bay, AK in the Beaufort Sea, in an ocean depth of approximately 3500m.

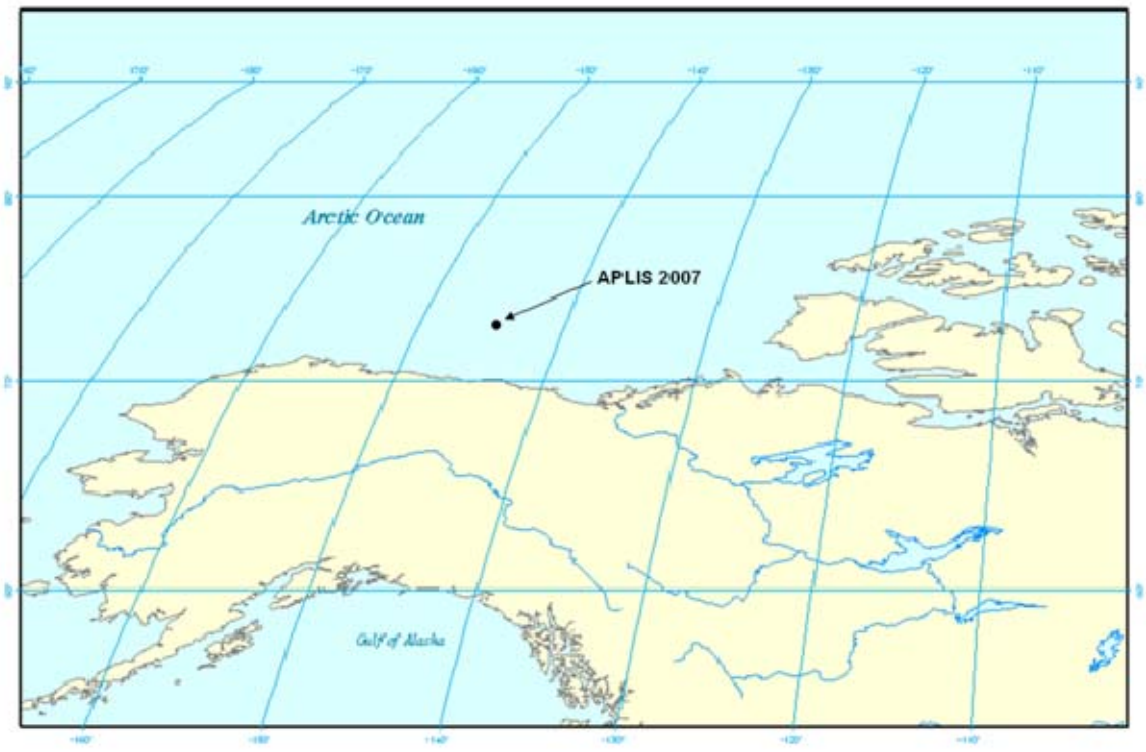

Figure 2. Location of Applied Physics Laboratory Ice Camp (APLIS).

The collection plan called for making under-ice current measurements on both sides of a selected ridge-keel structure and at multiple distances from the base of the ridge. The objective was to measure the turbulent wake generated by an ice keel. The

two ADVs were to be placed in the turbulent wake region of the boundary layer. Expected mean ice thickness was about 3m, as measured at two other locations on the floe.

Following arrival at Deadhorse, Alaska and briefing by U.S Navy Arctic Submarine Laboratory, a Cessna Caravan provided transportation to the ice camp. Upon arrival, the ice floe was surveyed to find a suitable ridge for the experiment. An old, multiyear ridge, located approximately 100m north of the camp, was selected as the experiment site. The ridge was the largest, most isolated and most linear within an allowable radius (defined by the U.S. Navy for safety reasons) from the camp. An 8 x 8 ft hut was constructed from which measurements would be made. On 16 March, a detailed topside survey of the pressure ridge and surrounding ice floe was conducted. The primary hole was melted 15m from the base of the ridge; this was expected to allow adequate distance from the keel to vertically sample the turbulent wake.

Figure 3. Applied Physics Laboratory Ice Station (APLIS).

The ADV was to be placed several meters below the ice on the tripod system and adjusted vertically periodically throughout the experiment to ensure that measurements were made in each of the flow regions discussed in Chapter II. With changing wind speed, the primary mechanism for forcing ice motion, the depth of the ADV would also be adjusted to see how changing ice motion affects the flow regimes.

On 17 March with the assistance of University of Washington personnel, the primary hydro hole was started. The melting process took three days and required melting through 12.5 meters of ice. As described above, it was hoped that other hydro holes would be melted further from the ridge base and on the opposite side of the ridge for additional collection opportunities, but the unexpected ice thickness and subsequent U.S. Navy submarine operations precluded melting any further holes, so the single hole had to serve for all the measurements.

Once the hole was cleared, the high frequency SONAR was deployed in hopes of mapping the underside of the ice and the selected ridge. As mentioned in Chapter III, noise problems precluded extensive surface mapping, but did yield some details of the under-ice surface within 5-7m around the hole which will be analyzed in future work in the context of the large scale structure measured by the Navy.

On 22 March the ADV was deployed and measurements were recorded for six days until the experiment concluded on 28 March.

THIS PAGE INTENTIONALLY LEFT BLANK

V. OBSERVATIONS AND DISCUSSION

Topside survey results show the selected pressure ridge height was 3.3m above sea level. The survey transects were interpolated into a surface representing the shape of the ridge. Because the ice keel's dimensions were not directly measured, the hydrostatic relationship was applied to estimate the depth. Based on local hydrostatic equilibrium and the pressure ridge height, and utilizing a sail height to keel depth ration of 1:3.2 (Davis and Wadhams, 1995), the dimensions of the keel were estimated in the absence of direct sub-ice measurements. Figure (4) shows a representation of what the keel might have looked like based solely on the above ratio.

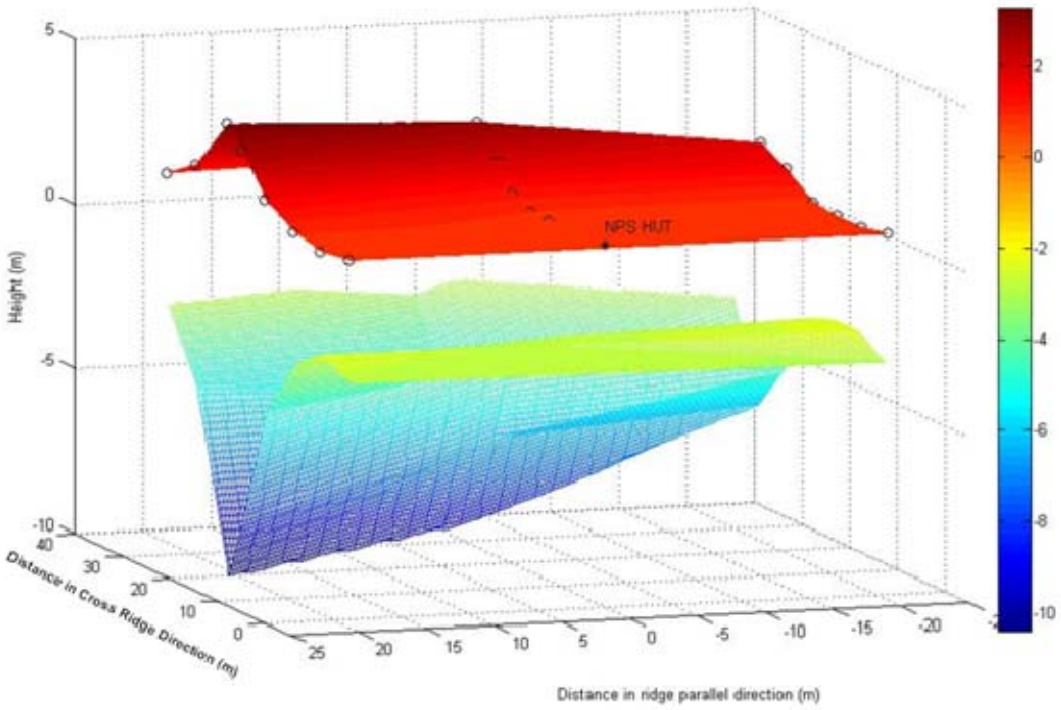

Figure 4. Results of topside ice ridge survey with notional ice keel estimated by hydrostatic relationships.

Clearly this was inaccurate since the keel was found to be much broader at least in the direction of our hut, where the ice extended 12.5m below sea level as measured through our hydro hole. A reasonable explanation would be that the ice rafted during the ridging process and that the hole was melted through that rafted slab of ice extending behind the ridge.

The ADV was initially deployed to a depth of 2.5m below the ice and following operability test, data collection began on 22 March. For the next three days, wind forcing was relatively low (Figure 5). Wind speed averaged less than 5 m/s and GPS derived ice motion averaged less than .05 m/s. Because of the light wind conditions, the ADV was kept in its position near the ice bottom, where it had the best opportunity to record the relatively small turbulence induced velocity perturbations. On 25 March (yearday 85) the wind increased to over 5 m/s resulting in ice speeds also increasing up to 0.2 m/s (Figure 5). In an effort to sample more of the boundary layer during the period of relatively high wind forcing, the ADV was lowered to 4.01 m and 5.52 m below the bottom of the ice hole. For the next 2.5 days, the high winds persisted and the ADV was alternated between 2.5, 4.0, and 5.5 meters below the ice collecting data in segments from ranging from 2 to 14 hours. It is these 2.5 days of relatively strong surface forcing that is the subject of the detailed analysis in the following discussions.

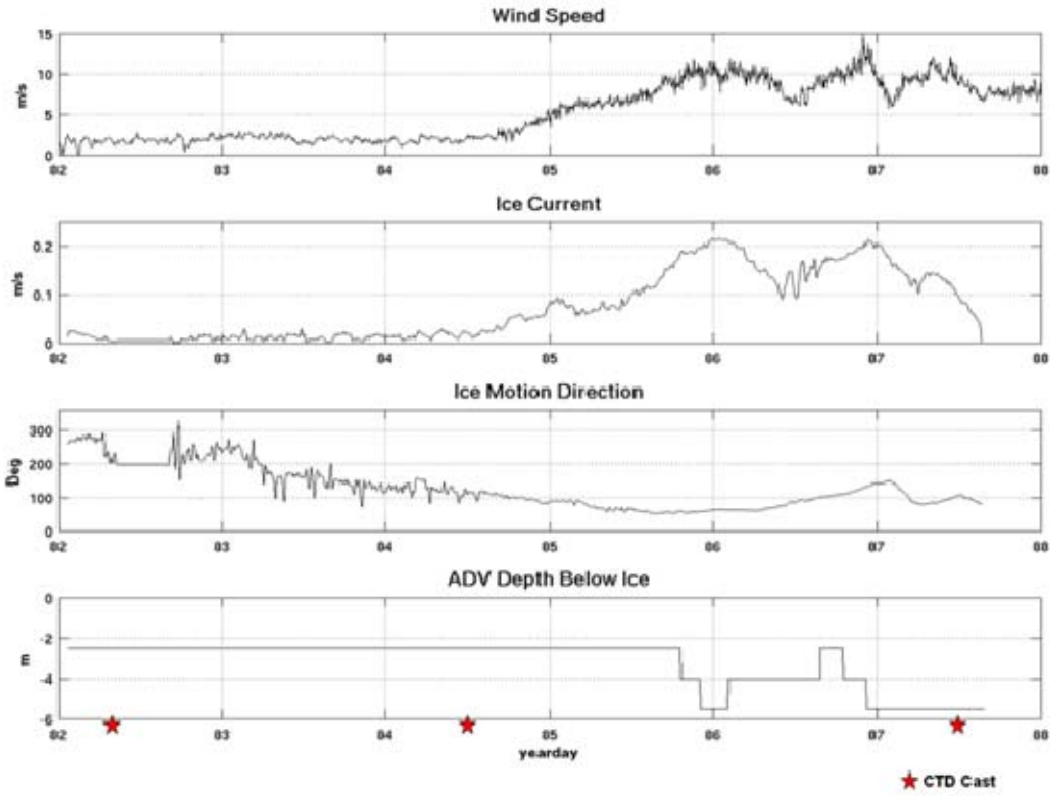

Figure 5. Plots of wind speed, ice speed, ice direction and deployed ADV depth. When the wind forcing increased around yearday 85 the ADV was deployed to different depths ranging from 2.5m to 5.5m in order to sample more of the boundary layer. Red stars indicate times of CTD cast.

Density profiles were calculated from the CTD data using equation of state formulations to estimate salinity from temperature and conductivity, and density from pressure, salinity, and temperature. Only three casts were made during the period of ADV operation, as indicated in Figure (5). Density profiles derived from those cast are presented in Figure (6).

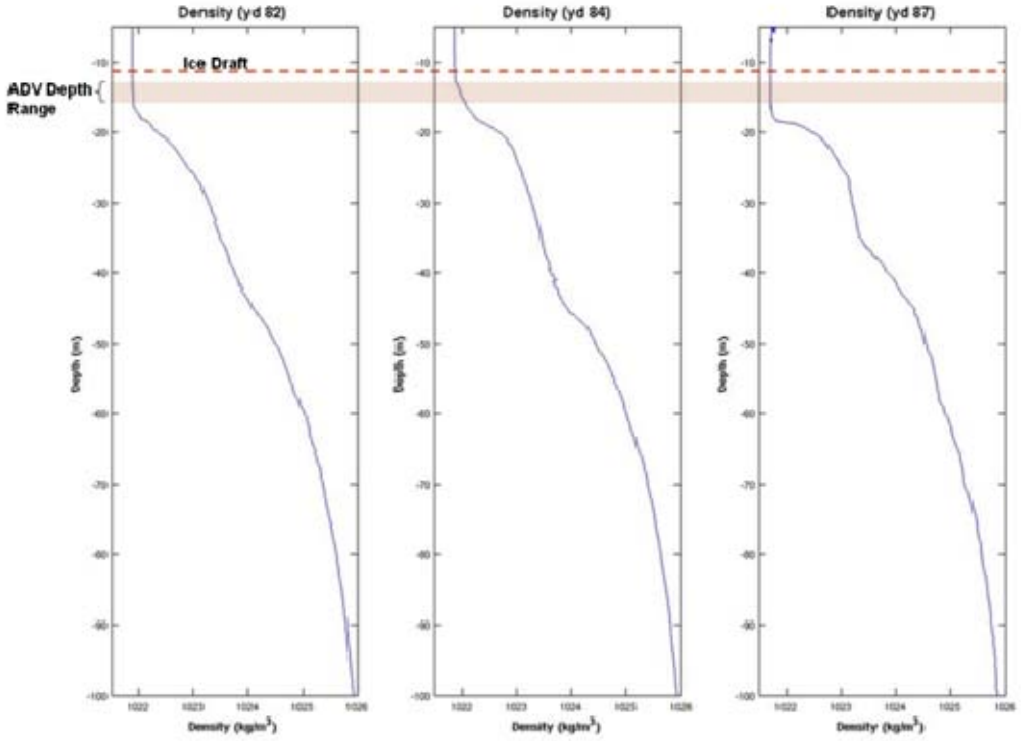

Figure 6. Density profiles from yearday 82 (left), 84 (middle), and 87 (right). Profiles show a relatively shallow mixed layer depth between 13-18m. The shallow mixed layer limits the boundary layer depth significantly and places the keel from which turbulence measurements were taken (12.5m deep) close to or in the pycnocline.

The strong, shallow stratification observed in Figure (6) was not expected and is attributed to the introduction of ice melt freshwater from widespread ice cover retreat observed the previous summer. The relatively shallow pycnocline and the exceptionally deep deployment of the ADV due to the thickness of the ice at the hydro hole make it reasonable to assume that the current measurements were made close to the bottom of the boundary layer and possibly into the salt stratified water column, below the turbulent boundary layer. Because periodic CTD measurements of the boundary layer depth were not permitted, inferences must be made from vertical velocity spectrum and the available profiles to determine when the ADV was within the boundary layer or in the stratification. To this end, it is expected that internal waves would be present on the

pycnocline, and their signature would be evident in the vertical velocity spectra and the $u'w'$ and $v'w'$ quadrature-spectra. To determine this, the buoyancy frequency, N was calculated using 2m differences of the density profiles (Figure 7).

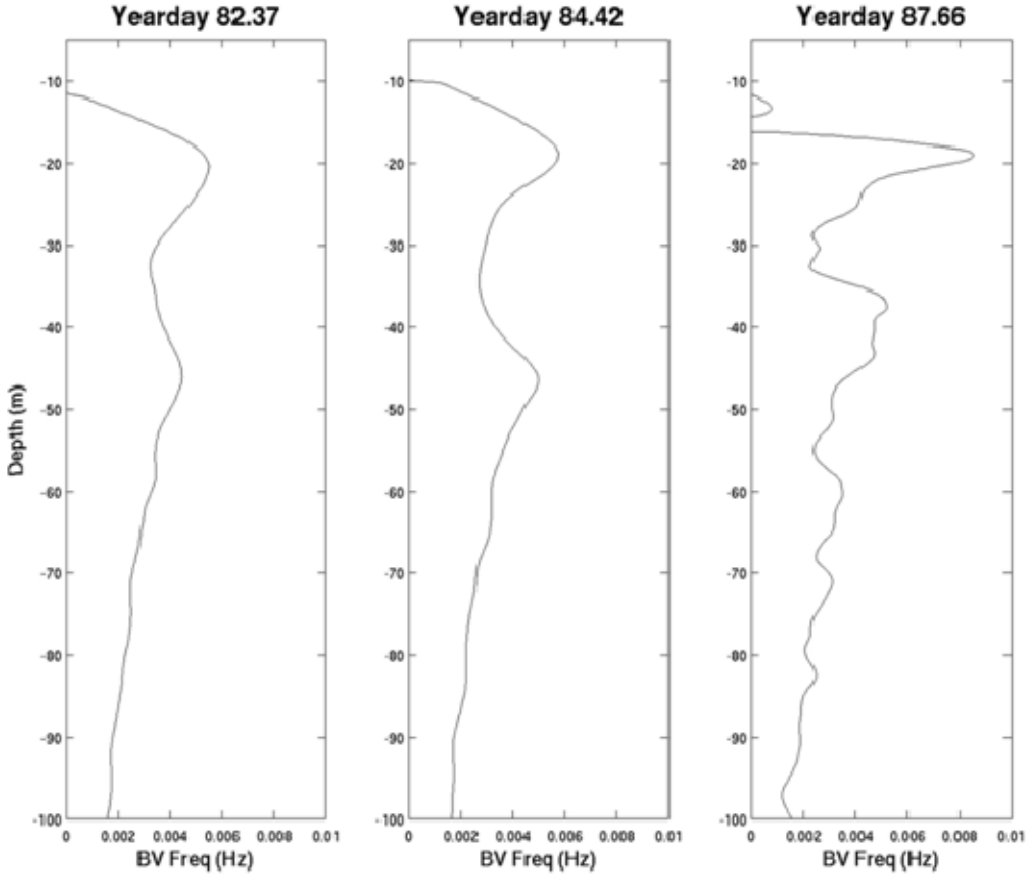

Figure 7. Buoyancy frequency calculated from density profiles from yearday 82, 84, and 87.

Velocity data from the SONTEK ADV was segmented into continuous time series of constant ADV depth, then cleaned via a de-glitching algorithm where the number of sequential points required to define the signal was set at 5, and the error threshold between sequential points of the velocity signal was set at .15 m/s for the horizontal components and .025 m/s for the vertical component. Additionally no more than 5% of the data would be discarded for cleaning purposes. The velocity components were rotated into along stream and cross stream components then broken into one hour ensembles for

analysis. Then, by removing the mean and linear trend, a time series of velocity perturbation values was calculated. The ADV data collected during the first two days of the experiment suffered from high noise resulting from very small signal levels due to low acoustic scatterer levels common in calm conditions. Much better data appeared after yearday 85.5 when the wind forcing resulted in much higher ice speeds indicated in Figure (5) and consistent backscatter amplitudes. For this reason, only data collected after yearday 85.5 is presented in this work.

Auto and cross spectra were calculated from the velocity perturbation in one hour ensembles. In order to better see the spectral characteristics, the log-averaged spectra were used where the spectrum data points were binned and averaged over 100 logarithmic bins spanning 0.001 to 2 Hz. Conversion from frequency space to wave number space for the purposes of calculating dissipation rates was done using Taylor's frozen field hypothesis where $k = \frac{2\pi f}{\overline{U}}$ and $\overline{U}$ is the measured mean horizontal fluid speed.

Three significant variables that are expected to significantly affect turbulent momentum flux estimates are ice current, which is the total speed of the ice as measured by GPS, ADV depth below the ice, and keel orientation relative to the mean direction of ice movement. For convenience of comparison, ADV depth, ice current and ice motion direction was also averaged over the same one hour periods.

Using ADV depth and ice current as criteria, the log averaged spectra for the vertical perturbation velocity, (S_{ww}), were sorted according to depth and ice speed and plotted together. ADV depth was at 2.5m, 4.0m, and 5.5m below the bottom of the ice. Ice ridge orientation was in the north-south direction (Figure 3) and it is expected that the general shape of the keel structure is orientated similarly. However, as evidenced from the depth of the hole, in comparison to the hydrostatic under-ice morphology (Figure 4), the actual under-ice morphology is probably more complicated, and the underside of the ice is likely a large rubble field. In this case, the local morphology of the keel near the ADV may have significantly more influence on the measured flow than the large scale keel structure.

Additionally, mean kinetic energy turbulent dissipation rates, ε, were calculated for each ensemble using the following relationship (Kundu, 1990):

$$Sww = \frac{12}{55}\alpha\varepsilon^{\frac{2}{3}}k^{\frac{-5}{3}}. \qquad (0.20)$$

The range of S_{ww} used to calculate the dissipation rate corresponds to the wave numbers where the inertial subrange is evident. Subtracted from S_{ww} is the estimated noise floor taken from each spectrum and α is the empirical Kolmogorov constant estimated at 1.56 (Shaw et al, 2001).

THIS PAGE INTENTIONALLY LEFT BLANK

VI. RESULTS

The complications imposed by the large roughness elements in combination with a relatively thin surface mixed layer imply that the standard approaches such as Arya (1975) proposed will not apply to this situation, therefore, it is evident that we did not measure the turbulent wake downstream of an isolated ice keel as originally planned. Without actual under ice imagery, it is not possible to know the keel surrounding the velocity measurements, however it is still relevant to examine measured turbulence through the water column near a very large structure at or near the pycnocline interface.

A. EFFECTS OF STRATIFICATION

Without adequate ocean profiling available to determine the depth of the mixed layer relative to measurement depth, an indirect approach was adopted. Analysis of the sorted, log-averaged spectra, S_{ww}, and associated dissipation rates allowed the proximity of the ADV to the pycnocline to be inferred. The pycnocline depth was determined from the profiles presented in Figure (6). Figure (8) shows dissipation rates plotted as a function of time along with the three independent variables: ice current, ice motion direction, and ADV depth.

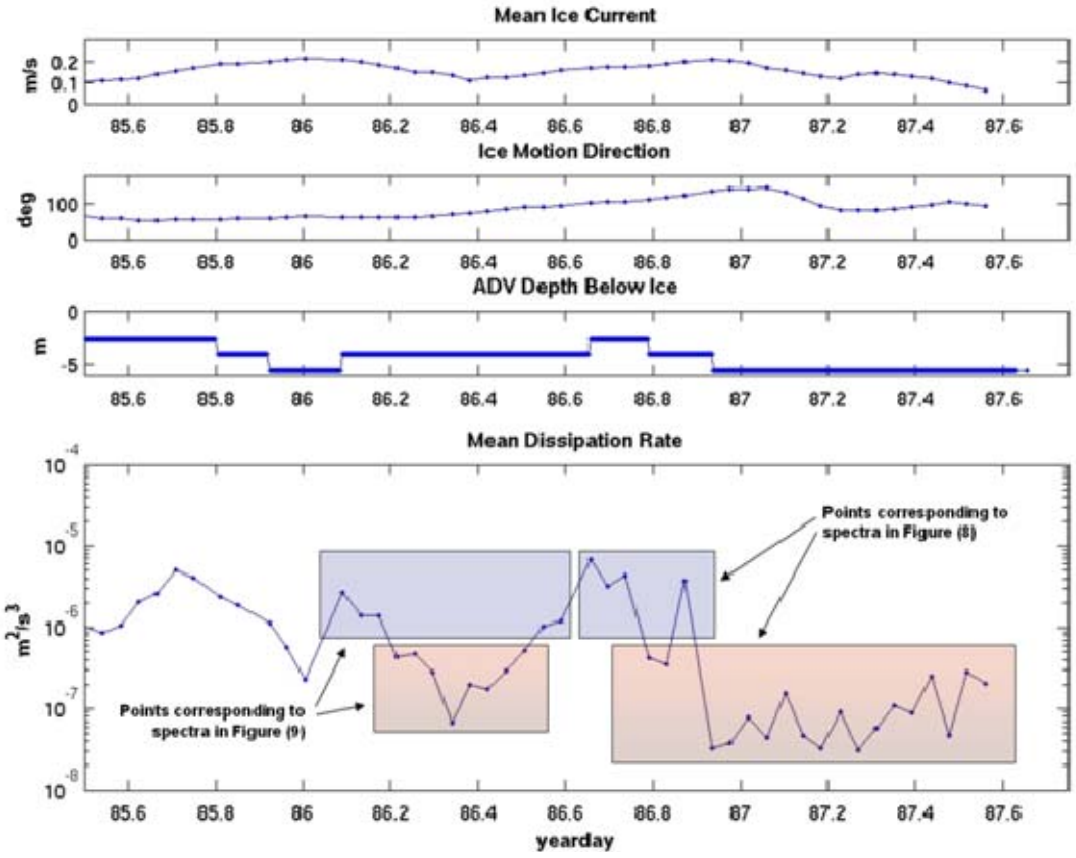

Figure 8. Mean turbulence dissipation rates calculated from one hour ensembles (bottom panel) plotted with ice current, direction and ADV depth (top three panels). Shaded regions in panel 4 indicate ensembles where corresponding spectra are calculated in Figures 9 and 10.

Around yearday 86.9 the significant drop-off in dissipation rates, by an order of magnitude, indicate that the ADV was very close or in the pycnocline. By inspecting the vertical velocity spectra from yearday 86.66 to yearday 87.60, (Figure 9), they appear similar at low frequencies but those spectra that correspond to ensembles with lower dissipation rates (plotted in red) fall off much faster through the inertial subrange than those with higher dissipation rates, plotted in blue. The same observations hold for measurements made from yearday 86.09 to 86.63 when the depth of the ADV was held constant at 4.0m below the ice. The difference in the inertial subrange energy levels in the vertical velocity spectra for this time period is shown in Figure (10).

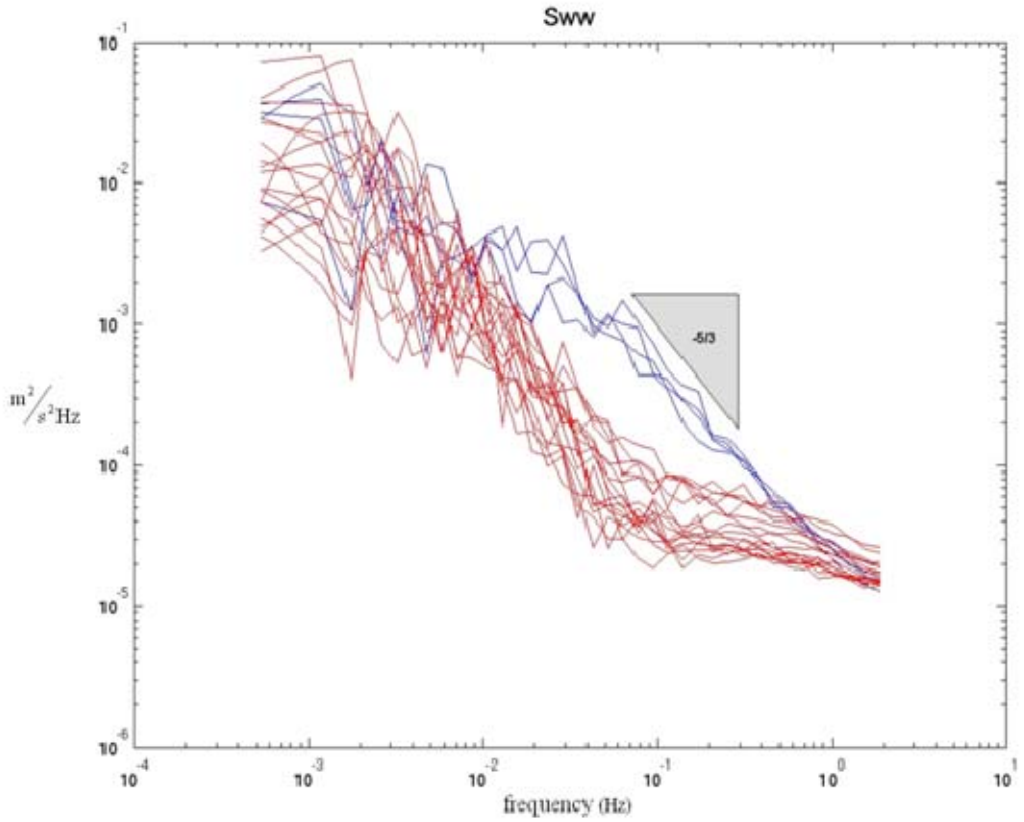

Figure 9. Vertical velocity spectra (S_{ww}) from yearday 86.66 to 87.60. Blue spectra indicate spectra calculated from yearday 86.66 to 86.78 and from 86.87 to 86.92. Spectra plotted in red were calculated for yearday 86.79 to yearday 86.87 and from 86.93 to 87.60. The -5/3rds slope is drawn in to highlight the turbulent inertial subrange.

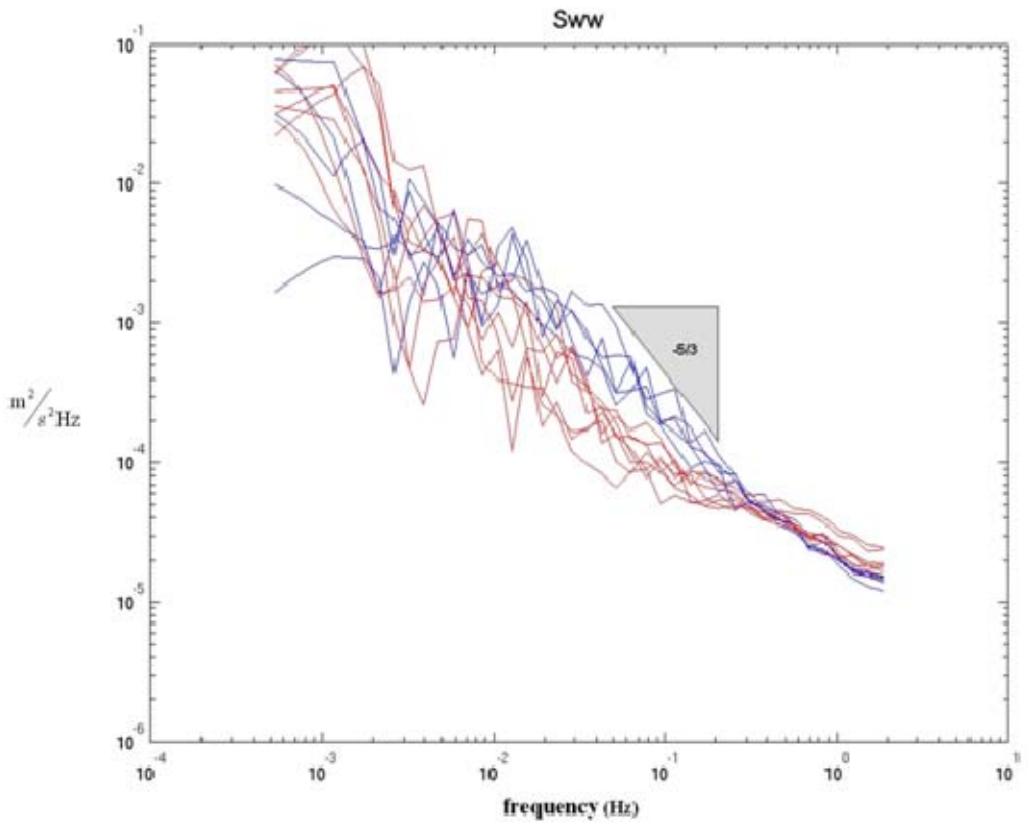

Figure 10. Vertical velocity spectra (S_{ww}) from yearday 86.09 to 86.63. Blue spectra indicate spectra calculated from yearday 86.09 to 86.21 and from 86.55 to 86.63. Spectra plotted in red were calculated for yearday 86.21 to yearday 86.55. The -5/3rds slope is drawn in to highlight the turbulent inertial subrange.

This effect may be caused by suppression of the turbulent eddies by stratification and would thus indicate when the proximity of the stratified layer has a significant effect on the measurements.

B. LOW FREQUENCY VARIANCE

The vertical velocity spectra also indicate that an unusually high level of variance at lower frequencies was present episodically. The observed low frequency variance was likely a result of either a wake effect caused by the under ice morphology or internal waves. To check for internal waves, the total quadrature spectra from $u'w'$ and $v'w'$ were summed over frequencies up to the buoyancy frequency. High levels of quadrature

energy in $u'w'$ and $v'w'$ relative to the co-spectral levels would indicate irrotational motion generally associated internal waves. This was not observed (Figure 11). Instead the quad and co-spectra levels were similar, which suggest a different mechanism with a turbulent character. A likely scenario is that this is the signature of a wake effect resulting from flow disturbance due to local under ice morphology. Due to the relatively shallow pycnocline, it is feasible that the flow around this under ice feature would also perturb the pycnocline creating a downstream internal wave signature, which is seen in the quad-spectra. Because this signal should only appear when the feature was upstream from the sensor relative to the ice motion, a directional dependence might be observed.

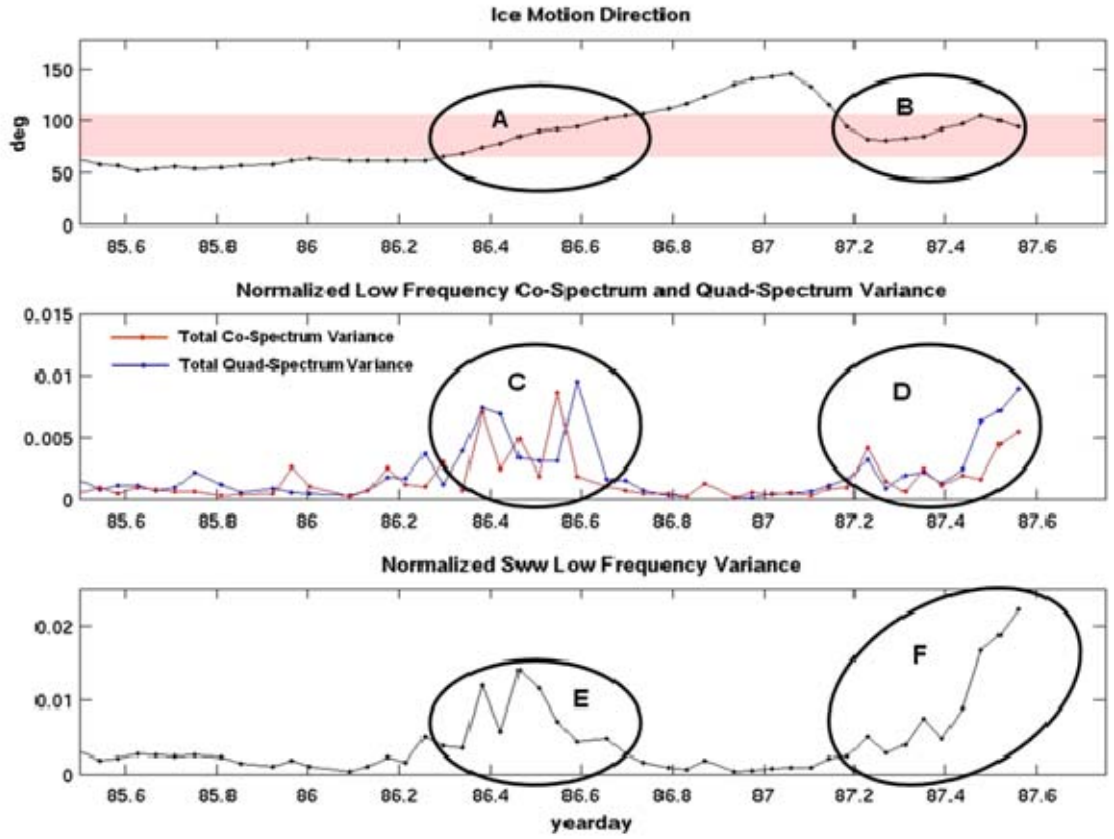

Figure 11. Ice motion direction is plotted in the top panel. Low frequency variance, normalized by the ice current (squared), for the quad and co-spectrum are plotted in the middle panel and the vertical velocity spectrum, (S_{ww}), in the bottom panel. Peaks in the variance, circled and labeled A through D, are observed to correspond to ice motion direction between 065° T and 105° T (shaded in red in top panel).

The co-spectra for $u'w'$ and $v'w'$ were analyzed in the same manner as the quad spectra (Figure 11). Peaks in the variance for both the co-spectra and quad-spectra are observed at similar times as indicated in region C and D and are coincident with time periods when the ice was moving roughly east, from $065°$ T through $105°$ T, indicated in regions A and B. These peaks also correspond to times when high variance was observed at low frequency in the vertical velocity spectra as indicated in region E and F.

Given the assumption that measurements are being made in a large ice rubble field with ice structures reaching to, at least, within meters of the relatively shallow and strong pycnocline, and the apparent dependence on ice motion direction, the observed low frequency variance is very likely the result of a wake effect resulting from the flow around an upstream ice feature in the $065°$ T to $105°$ T quadrant.

C. STRESSES

Turbulent stresses were analyzed in terms of friction velocities given by (1.15). Figure (12) shows time series of mean ice current, direction and ADV depth with friction velocities plotted in the bottom panel.

Interface friction velocity estimates based on Rossby similarity theory (Shaw et al, 2007) were calculated to provide a basis for comparison to actual friction velocities calculated from measured velocities. These estimates are based on observed ice speed, a 10cm roughness length and a relatively deep boundary layer which represent more typical ice conditions. Actual friction velocities were calculated using two methods resulting in a total friction velocity and a filtered friction velocity. The total friction velocity was calculated directly from the perturbation velocities using equation (1.15) and represents contributions from both boundary driven shear stress and local wake generated stress. Filtered friction velocities were calculated from the summed variance of the high passed filtered co-spectra for $u'w'$ and $v'w'$. Half the buoyancy frequency was used as the filtering cutoff frequency which was observed to be 2.9×10^{-3} Hz. The filtered friction velocities are meant to represent contributions only by boundary shear generated stresses.

The difference between the total friction velocities and the high pass filtered friction velocities should then be representative of the contribution of wake generated stresses.

It is most likely that measurements were made in a large rubble field where roughness lengths are greater than 10cm, and the observed shallow pycnocline significantly limited the boundary layer depth; therefore, it is improbable that the measurements were made under small roughness element under-ice conditions.

Unfiltered friction velocities show significant variation (Figure 12). As discussed above, local ice morphology is likely responsible for a wake effect that appears as low frequency energy in the velocity spectra and probably is responsible for some of this temporal variation.

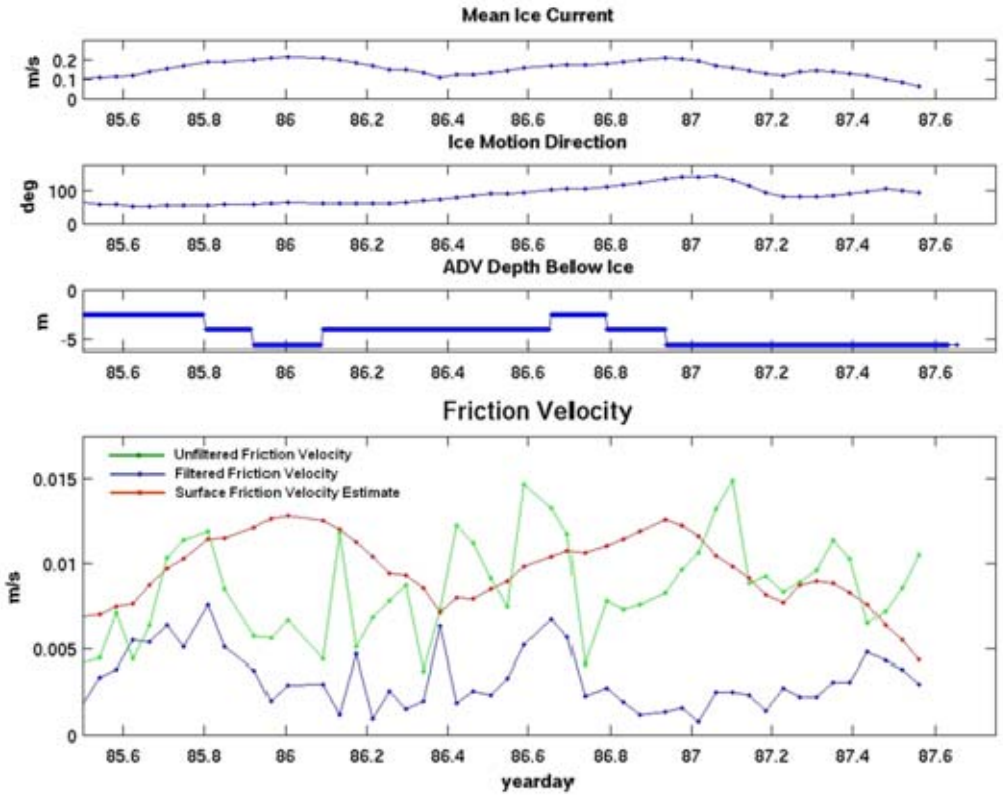

Figure 12. Observed mean ice current, direction and ADV depth plotted in top three panels. In the bottom panel are friction velocities calculated from one hour ensembles in green and blue. Estimates of under ice surface friction velocities based on observed ice current and a 10cm roughness length in red. The friction velocities plotted in green are calculated from unfiltered velocities while those plotted in blue have been high passed filtered based on half the observed buoyancy frequency to remove low frequency signals.

The filtered friction velocities, representing only the boundary shear driven turbulent stresses, are much smaller than the surface friction velocities predicted by Rossby similarity theory in an area of assumed large roughness elements. This may be due to two separate effects. As previously discussed, the pycnocline is very shallow and the deep draft of the ice results in observations being made close to the pycnocline. Turbulent stresses diminish towards the bottom of the boundary layer (Smith et al, 1990), thus the proximity of the pycnocline explains, at least partially, the smaller observed stresses. Additionally, and more speculative, is the possibility that given the complicated under-ice morphology, the ADV may have been positioned near enough to a large under-ice formation to be in a separated flow region, such as indicated by region 4 in Figure (1). In this area, the mean flow is disrupted and turbulent stresses are expected to be smaller than in regions outside of the separated flow. The low frequency component of the stress is as large as the 10cm roughness length Rossby similarity theory estimate indicating, at least in this one position, the "wake-like" effect is significant in terms of momentum transport.

VII. SUMMARY

A detailed analysis of under ice turbulence measurements taken at a single point during APLIS 2007 has been presented. The data spanned several days and is taken in an ice environment consisting of an exceptionally large ice draft and a relatively shallow pycnocline, resulting in measurements made in close proximity to the stratified layer. The turbulence data show a strong dependence on ice current speed, ice motion direction and the measurement depth below the ice.

Measured stresses showed a directionally dependent low frequency component that is likely the result of a wake effect generated by a large, local under-ice feature. The high levels of low frequency energy observed in the velocity spectra may be rotational eddies shed off of the wake that have not yet formed a well-developed inertial subrange. The diminished inertial subrange evident in the velocity spectra may represent the integrated background stresses of the under-ice ocean boundary layer. Because these boundary layer stresses were measured in close proximity to the pycnocline, this might explain the low stress levels we observed.

Detailed ice topography will provide a more complete context for these turbulence observations, and is expected to become available for this area in the future. This is anticipated to greatly aid in understanding the turbulent effects described in this paper.

THIS PAGE INTENTIONALLY LEFT BLANK

LIST OF REFERENCES

Arya, S. P. S. (1975), A drag partition theory for determining the large-scale roughness parameter and wind stress on the arctic pack ice, *J. Geophys Res.*, 80, 3447-3454.

Bourke, R. H., and A. S. McLaren (1992), Countour mapping of the Arctic Basin ice drift and roughness parameters, *J. Geophys Res.*, 97, 17,715-17,728.

Davis, N. R., and P. Wadhams (1995), A statistical analysis of arctic pressure ridge morphology, *J. Geophys Res.*, 100, 10,915-10,925.

Kundu, P. K., (1990), *Fluid Mechanics*, pp. 441-442, Academic Press, San Diego.

Marshall, J. K. (1971), Drag measurements in roughness arrays of varying density and distribution, *Agricultural Meteorology*, 8, 269-292.

McPhee, M. G., (1990), Small scale processes. in *Polar Oceanography*, edited by W. Smith, pp. 287-334, Academic Press, San Diego.

Shaw, W. J., J. H. Trowbridge, and A. J. Williams III, (2001), Budgets of turbulent kinetic energy and scalar variance in the continental shelf bottom layer, *J. Geophys Res.*, 106, 9551-9564.

Shaw, W. J., T. P. Stanton, M. G. McPhee, and T. Kikuchi, (2007), Estimates of surface roughness length in heterogeneous under-ice boundary layers, accepted for publication in *J. Geophys Res*.

Unesco, (1981), Background papers and supporting data on the International Equation of State of Seawater 1980. *Unesco Technical Papers in Marine Science*, No. 38, 192.

Whelan, J. Q., W. Maslowski, J. L. Clement Kinney, and J. Jakacki, (2007), Understanding Recent Variability in the Arctic Sea Ice Thickness and Volume - Synthesis of Model Results and Observations, AGU, 88(52) Fall Meet. Suppl., Abstract C22A-06.

THIS PAGE INTENTIONALLY LEFT BLANK

INITIAL DISTRIBUTION LIST

1. Defense Technical Information Center
   Ft. Belvoir, Virginia

2. Dudley Knox Library
   Naval Postgraduate School
   Monterey, California

3. Dr. Mary L. Batteen
   Naval Postgraduate School
   Monterey, California

4. Prof. Timothy Stanton
   Naval Postgraduate School
   Monterey, California

5. Dr. William Shaw
   Naval Postgraduate School
   Monterey, California

6. Dr. Wieslaw Maslowski
   Naval Postgraduate School
   Monterey, California